Engineering 4 (2018) 676–684

Contents lists available at ScienceDirect

Engineering

journal homepage: www.elsevier.com/locate/eng

Research
Applied Geophysics—Article

Spatial Discrimination of Complex, Low-Relief Quaternary Siliciclastic Strata Using Airborne Lidar and Near-Surface Geophysics: An Example from the Texas Coastal Plain, USA

Jeffrey G. Paine *, Edward W. Collins, Lucie Costard

Bureau of Economic Geology, Jackson School of Geosciences, The University of Texas at Austin, Austin, TX 78713, USA

ARTICLE INFO

Article history:
Received 11 November 2017
Revised 24 April 2018
Accepted 7 September 2018
Available online 15 September 2018

Keywords:
Lithology
Geophysics
Electromagnetic induction
Lidar

ABSTRACT

Depositional units preserved on coastal plains worldwide control lithologic distribution in the shallow subsurface that is critical to infrastructure design and construction, and are also an important repository of information about the large-scale climate change that has occurred during many Quaternary glacial-interglacial cycles. The lateral and vertical lithologic and stratigraphic complexity of these depositional units and their response to climatic and sea-level change are poorly understood, making it difficult to predict lithologic distribution and to place historical and future climate and sea-level change within a natural geologic context. Mapping Quaternary siliciclastic depositional units on low-relief coastal plains traditionally has been based on their expression in aerial photographs and low-resolution topographic maps. Accuracy and detail have been hindered by low relief and lack of exposure. High-resolution airborne lidar surveys, along with surface and borehole geophysical measurements, are being used to identify subtle lateral and vertical boundaries of lithologic units on the Texas Coastal Plain within Quaternary strata. Ground and borehole conductivity measurements discriminate sandy barrier island and fluvial and deltaic channel deposits from muddy floodplain, delta-plain, and estuarine deposits. Borehole conductivity and natural gamma logs similarly distinguish distinct lithologic units in the subsurface and identify erosional unconformities that likely separate units deposited during different glacial-interglacial stages. High-resolution digital elevation models obtained from airborne lidar surveys reveal previously unrecognized topographic detail that aids identification of surface features such as sandy channels, clay-rich interchannel deposits, and accretionary features on Pleistocene barrier islands. An optimal approach to identify lithologic and stratigraphic distribution in low-relief coastal-plain environments employs ① an initial lidar survey to produce a detailed elevation model; ② selective surface sampling and geophysical measurements based on preliminary mapping derived from lidar data and aerial imagery; and ③ borehole sampling, logging, and analysis at key sites selected after lidar and surface measurements are complete.

1. Introduction

Broad, low-elevation, and low-relief plains composed of complex assemblages of Quaternary siliciclastic sediments (dominantly sand, silt, clay, and gravel) are common along the passive oceanic margins of all continents. These unconsolidated to semi-consolidated sediments, which are the depositional record of terrestrial and marine sedimentary processes active during multiple glacial and interglacial climatic cycles of the Quaternary period, serve as the natural foundation for the infrastructure of thousands of coastal cities, smaller communities, and other coastal industrial, residential, and recreational facilities. It is thus important from an engineering as well as a geological perspective to better characterize the lithology and spatial distribution of these siliciclastic strata in the shallow subsurface in order to enable improved siting and design of engineered structures and to document the response of coastal depositional systems to large-scale changes in sea level associated with past climate change. Lessons learned from coastal response to past climatic change can inform possible geologic response to future change.

* Corresponding author.
E-mail address: jeff.paine@beg.utexas.edu (J.G. Paine).

https://doi.org/10.1016/j.eng.2018.09.005

We are employing airborne lidar surveying to produce high-resolution digital elevation models (DEMs) of a low-relief coastal plain in order to enable the identification of subtle topographic expressions of lithologic change that are associated with sandy paleochannels, muddy overbank and delta-plain deposits, and sandy and muddy deposits of Pleistocene barrier islands and associated bays and lagoons. Depositional environments and lithologies inferred from DEMs and imagery can be confirmed and further delineated laterally using ground-surface measurements of electrical conductivity, because electrical conductivity is strongly correlated to clay content [1]. Depths and thicknesses of major lithologic units can be estimated from electrical conductivity data acquired using time-domain electromagnetic induction (TDEM) measurements at the ground surface, and can be further subdivided where necessary with borehole geophysical logs. Two useful borehole tools are ① electromagnetic induction (EM), which can be used to measure the electrical conductivity of subsurface strata in open or plastic tubing-cased boreholes and water wells, and ② natural gamma ray activity, which increases with clay content in most siliciclastic environments. We applied this approach on the central Texas Coastal Plain, which is part of a passive continental margin along the northwestern Gulf of Mexico (Fig. 1) [2]. This approach is applicable to similar siliciclastic coastal plains worldwide.

The Texas Coastal Plain is underlain by a complex assemblage of fluvial, deltaic, estuarine, and marine-influenced deposits that make up two principal Pleistocene formations (Fig. 1): the younger Beaumont Formation and the older Lissie Formation [3–11]. These two formations record depositional, erosional, and weathering events associated with more than 20 full or partial glacial-interglacial cycles that are recorded in ice and sediment cores worldwide, as mentioned in Refs. [12–17]. Surface, borehole, and geophysical data from diverse sources suggest that the strata within these two formations represent multiple episodes of deposition, erosion, and soil formation.

Much of the original mapping of geological units on the Texas Coastal Plain was based on the interpretation of early aerial photographs, agricultural usage, low-resolution (1.5 m contour interval) topographic maps, and limited exposures in stream valleys and along bay shorelines. In this paper, we employ ① high-resolution topography as determined from an airborne lidar instrument (elevations accurate to a few centimeters) to map the subtle topographic expressions of Quaternary depositional and erosional features; ② ground-based electrical conductivity measurements to distinguish and delineate the lateral and vertical extent of sand-rich and clay-rich depositional units at and near the surface; and ③ subsurface sampling and borehole-based gamma ray activity and electrical conductivity measurements to determine vertical lithologic boundaries, erosional unconformities, and buried soil horizons that are generally below the resolution of surface and airborne geophysical approaches. We are using these data to produce geologic maps of the coastal plain; to determine the depth, thickness, and character of near-surface lithologic units; and, eventually, to better understand the relationship between depositional units, unconformities, and soil horizons within the Quaternary strata and the numerous climatic and sea-level cycles that occurred during their deposition. This paper focuses on recent work on the central Texas coast in the Corpus Christi Bay, Copano Bay, San Antonio Bay, and Matagorda Bay areas (Figs. 1 and 2).

2. Methods

We combined high-resolution topographic data acquired using an airborne lidar instrument, surface and borehole geophysical measurements, and select surface and borehole sediment samples to help delineate the lateral and vertical extent of Quaternary lithologic units on the central Texas Coastal Plain. Airborne lidar data were acquired between 2013 and 2016 in the Copano Bay area, the San Antonio Bay area, and the Matagorda Bay area using a Chiroptera airborne lidar instrument (Airborne Hydrography AB, Jönköping, Sweden) operating at a laser pulse rate of 100–200 kHz and a flight height of 440–1000 m [18]. Global positioning system (GPS) data from survey-area base stations were combined with aircraft-based GPS and inertial navigation-system data to produce highly accurate instrument trajectories that, when combined with laser orientation and travel-time information, allowed the determination of absolute surface reflection positions that were accurate to within a few centimeters. Laser returns were binned to produce a high-resolution DEM of the area using a 1 m × 1 m cell size.

We used frequency-domain electromagnetic induction (FDEM) and TDEM methods to measure apparent conductivity from the ground surface to depths of 100 m or more in the study area. FDEM methods employ a changing primary magnetic field created around a transmitter coil to induce current to flow in the ground or in the annulus around a borehole, which in turn creates a secondary magnetic field that is sensed by the receiver coil [19–21]. The strength of the secondary field is a complex function of EM frequency and ground conductivity [22], but generally increases with ground conductivity at constant frequency. TDEM devices measure the decay of a transient, secondary magnetic field produced by eddy currents that are induced to flow in the ground by the termination of a primary electric current flowing in a transmitter loop [23,24]. The secondary field strength is measured by the receiver coil at discrete time intervals following transmitter current termination. In horizontally layered media, secondary field strength at early times gives information on conductivity in the shallow subsurface; field strength at later times is influenced by conductivity at depth.

Ground-based apparent conductivity measurements were acquired on the central Texas Coastal Plain (Fig. 2) using Geonics EM38 (366 sites) and EM31 (421 sites) ground conductivity meters in horizontal and vertical dipole orientations. These FDEM instruments measure apparent conductivity from the surface to depths

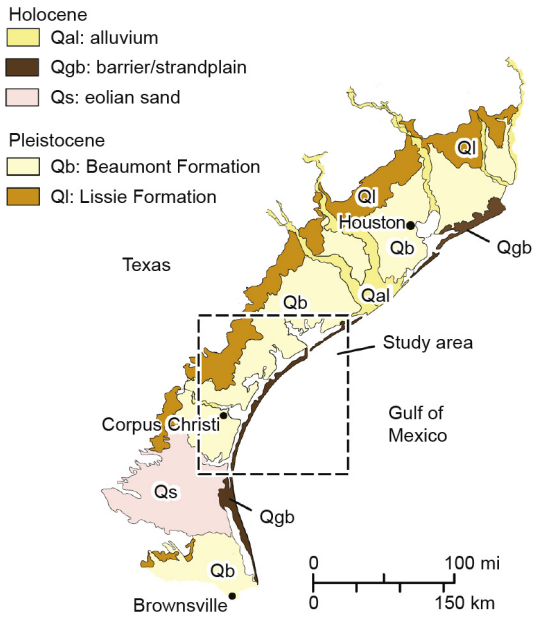

Fig. 1. Schematic diagram showing the principal Quaternary geologic units on the Texas Coastal Plain and the central Texas coast study area in the southern United States. (Adapted from the Bureau of Economic Geology [2])

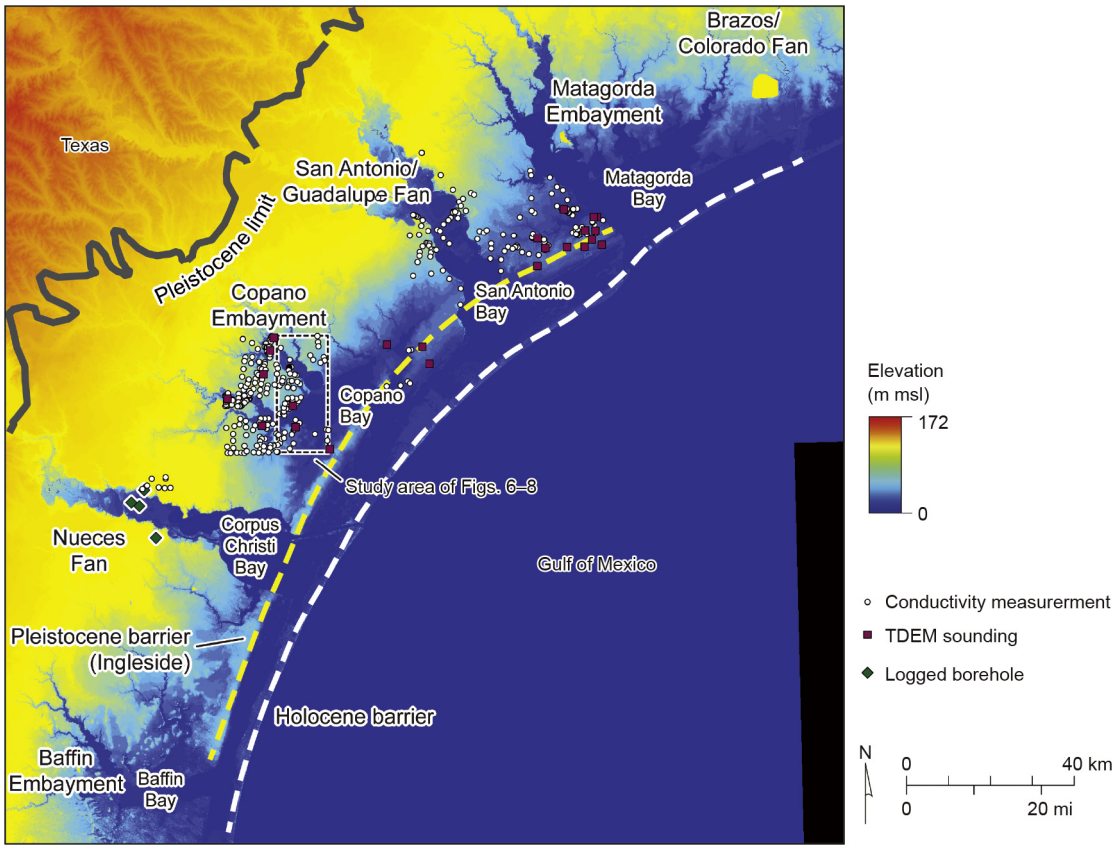

Fig. 2. DEM (100 m^2 cell size) of the central Texas Coastal Plain (Fig. 1) and the Copano Bay study area (dashed rectangle). Also shown are late Quaternary geologic features (fans, embayments, bays, and barrier islands) and locations of logged boreholes, frequency-domain electromagnetic induction (FDEM) conductivity measurements, and TDEM soundings. msl: mean sea level. (DEM from the US Geological Survey)

that depend on the primary frequency of the transmitter, the transmitter and receiver coil separation distance, and the conductivity of the ground [22]. The EM38 operates at a primary frequency of 14 600 Hz with a transmitter and receiver coil separation of 1.0 m. Exploration depth for the EM38 is about 0.7 m in horizontal dipole orientation and about 1.5 m in vertical dipole orientation. The EM31 operates at a primary frequency of 9800 Hz with a transmitter and receiver coil separation of 3.7 m. Exploration depth is 3 m or less in horizontal dipole mode and 6 m or less in vertical dipole mode. Together, these instruments are adequate to measure the electrical conductivity (and, by proxy, to provide a measure of clay content) of most surficial lithologic units identified through their expression on high-resolution DEMs and imagery.

TDEM data were acquired at 23 sites on the coastal plain (Fig. 2). At three sites, we acquired TDEM data using a terraTEM instrument (Monex GeoScope Pty Ltd., The Basin, VIC, Australia) with a 40 m × 40 m transmitter and receiver loop, 3–8 A transmitter current, and turnoff times ranging from about 14 to 27 μs. At the remainder of the sites, we acquired data using a WalkTEM instrument (ABEM Instrument AB, Sundbyberg, Sweden) using either a square 40 m × 40 m transmitter loop or a circular transmitter loop with a 25.5 m radius. The circular loop is preferred because it is easier to deploy and gives a 25% larger dipole moment for the same transmitter current and loop length, potentially yielding greater signal-to-noise ratio and exploration depth. The WalkTEM instrument has the capability to record transient signals generated during a high-moment transmitter pulse (about 8 A transmitter current) to maximize exploration depth, and a low-moment transmitter pulse (about 1 A transmitter current) to maximize resolution in the shallow subsurface. These data are acquired simultaneously and are jointly inverted to produce layered or smooth conductivity models that fit the observed transient decays generally within one or two percent of what the modeled response would be. TDEM data were used to determine generalized subsurface conductivity profiles to depths of 100 m or more, which allowed estimation of sandy and clayey unit thicknesses and depths.

Direct observation of the shallow subsurface was achieved by drilling and sampling new boreholes and geophysically logging new boreholes and older water wells. Four boreholes were drilled to depths of about 30 m in the Nueces River valley upstream from Corpus Christi Bay (Fig. 2) to examine lithologic characteristics and the relationship among sediment texture, as measured in the laboratory, and *in situ* geophysically logged parameters including gamma ray activity and apparent conductivity. Sediment was described and sampled during drilling at about 1.5 m intervals using a split-spoon sampler. Upon reaching total depth, the boreholes were temporarily cased using polyvinyl chloride (PVC) pipe and logged using spectral gamma and induction tools (2SNA-1000-S and 2PIA-1000; Mount Sopris Instruments Inc., Denver, CO, USA) that measured gamma ray activity and apparent conductivity at intervals of 5 cm in the boreholes. Fifteen older water wells have been logged on the coastal plain using the gamma and induction tools. These logs were acquired in PVC-cased water wells that were 32–92 m deep. Neither sediment samples nor lithologic descriptions were available for these wells, but the gamma and conductivity logs provided detailed, site-specific data on the vertical distribution of sands, clays, and mixed siliciclastic units for comparison with conductivity profiles derived from TDEM data.

We acquired surface and borehole sediment samples in the study area for textural analysis and comparison with surface- and borehole-based geophysical measurements. In the laboratory, a representative fraction (0.2–0.5 g) was taken from each sample and placed in a tube. Sediments were dispersed by adding 5% sodium hexametaphosphate solution, shaken for 24–48 h, and passed through a 2 mm (#10) sieve. The particle-size distribution of the passing suspension was determined by laser light diffraction using a Mastersizer 3000 (Malvern Instruments Ltd., Malvern, UK) laser particle-size analyzer, cycling through the measurement five times to improve size-distribution statistics.

3. Relationship among sediment texture, gamma ray activity, and conductivity

Data from the four boreholes drilled across the Nueces River valley upstream from Corpus Christi Bay (Fig. 2) illustrate the complementary nature of geophysical measurements and direct geological observations. In borehole ND-06, which was drilled to a depth of about 30 m on the floor of the Holocene Nueces River delta at a surface elevation of 1.5 m above mean sea level (msl), it is evident that the gamma log (Fig. 3(a)) correlates quite well qualitatively with the clay content in borehole samples acquired at 1.5 m intervals (Fig. 3(b)). High gamma counts (20 counts·s^{-1} or higher) correspond to high clay contents, suggesting that the gamma log is a reliable proxy for clay content and can be used to distinguish sand-rich and clay-rich units. In this example, unit thicknesses determined from the gamma log range from 1 m or thinner to greater than 5 m, showing both abrupt lithologic boundaries and gradational ones.

The conductivity log (Fig. 3(c)) has a character similar to the gamma log and textural trends in the upper 15 m; higher conductivities in the upper half of the log correlate with higher gamma counts and higher clay content. Below 15 m depth, apparent conductivity decreases significantly and does not correlate well with gamma or textural trends. The most likely interpretation is that the upper part of the conductivity log is influenced by highly saline pore water at a nearly constant concentration. At depths greater than about 17 m, pore-water salinity progressively diminishes with depth; the concentration reduction dominates the conductivity response in these water-saturated strata. It is evident from this example that there are limitations to using conductivity measurements exclusively to develop an accurate subsurface lithologic framework, particularly in areas having high-salinity pore water.

The relationship between sediment texture and geophysical log response can be evaluated to a limited degree by directly comparing sediment texture determined from borehole samples to *in situ* geophysical measurements of gamma ray activity and apparent conductivity recorded using borehole tools at approximately equivalent depths. Because samples were acquired with a split-spoon sampler during borehole drilling, sample depths are only approximately accurate. Geophysical measurements made by borehole instruments reveal reasonably continuous variations that correspond to lithologic (texture and mineral composition) changes with depth; however, these measurements represent average values for the stratal depth range and sensing volume around the borehole.

From the four boreholes that were both sampled and logged, we acquired 92 samples that were available for comparison with geophysical measurements. Of these, 88 samples had both textural analyses and gamma ray activity measurements at similar depths. Because of the length of the borehole tools, four samples were acquired at depths greater than the depth logged by the borehole instruments and could not be compared to geophysical measurements. The general similarity of patterns between the textural measurements and the gamma logs of an individual borehole (e.g., Fig. 3) suggests that gamma ray activity increases with clay content; however, when samples and logs from all four boreholes are combined, the relationship is weaker than expected (coefficient of determination R^2 = 0.22, Fig. 4). Possible reasons for this include ① depth mismatches between sample depths and borehole log depths, ② lateral and vertical sediment heterogeneity, and ③ incomplete disaggregation of clay in the sediment samples during textural analysis. In these boreholes, the continuous gamma log is a better indicator of vertical change in clay content than the textural data from limited borehole samples.

Textural and geophysical log data from borehole ND-06 (Fig. 3) show a relationship between apparent conductivity and clay content over only the upper part of the borehole. At greater depths, change in pore-water salinity more strongly influences apparent conductivity than does textural change. Most apparent conductivity measurements taken at the ground surface on the coastal plain sense strata that are above the water-saturated zone, where

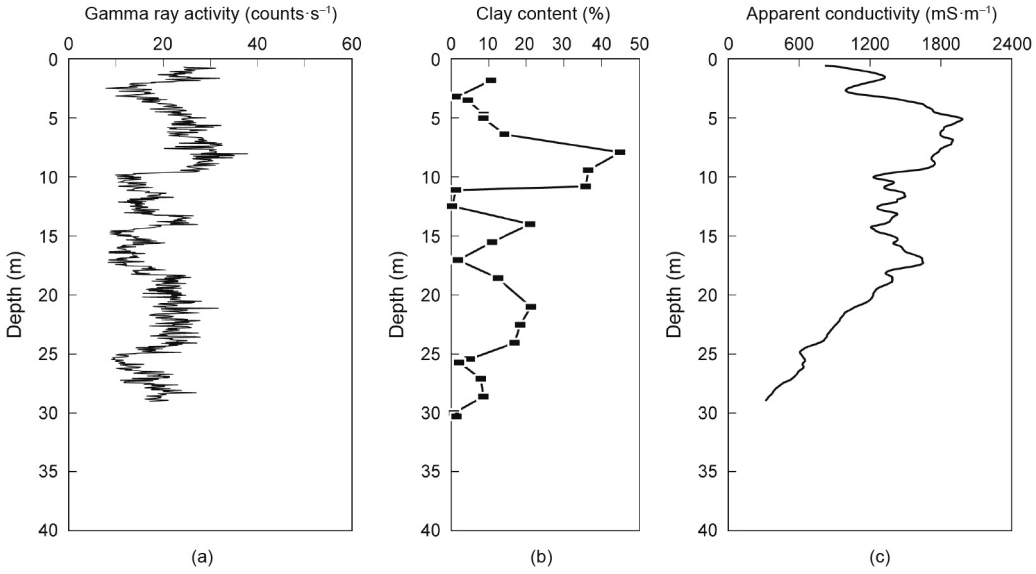

Fig. 3. (a) Gamma ray activity, (b) clay content, and (c) apparent conductivity from borehole ND-06 on the Nueces River delta upstream from Corpus Christi Bay (Fig. 2).

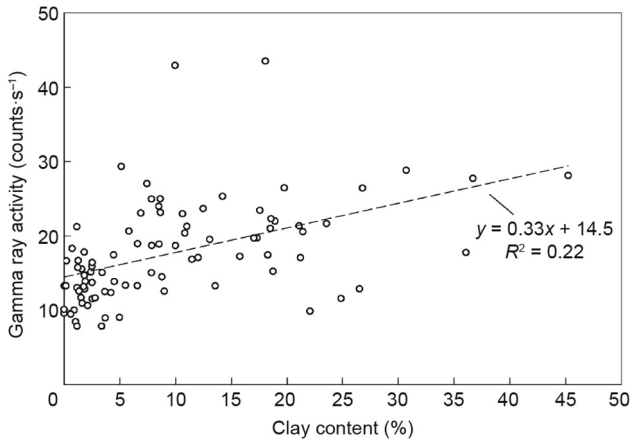

Fig. 4. Relationship between clay content (determined from borehole samples) and gamma ray activity (from geophysical logs) from two boreholes on the floor of the Nueces River valley and two boreholes on the Pleistocene surface adjacent to the valley (Fig. 2).

textural and mineralogical changes more strongly influence conduction of electrical currents [25]. To examine this relationship, we compared borehole apparent conductivity measurements with laboratory-measured clay content from samples from the boreholes at depths above the water-saturated zone, principally from the two boreholes situated on the upland adjacent to the Nueces River valley. This restriction yielded 28 samples for comparison with conductivity log response. The relationship between clay content and apparent conductivity measured *in situ* at approximately equivalent depths is stronger (coefficient of determination $R^2 = 0.84$, Fig. 5) than that between gamma ray activity and clay content, suggesting that measurements of apparent conductivity can serve as a reasonable proxy for clay content where water saturation of sediment and pore-water salinity are low, or perhaps reasonably constant throughout the logged depth range.

4. Geomorphology and surficial lithologic distribution from high-resolution DEM

To illustrate the approach to mapping distinct lithologic units and determining lithologic properties and lateral and vertical distribution, we show data from an area encompassing two 7.5 min quadrangles on the western margin of Copano Bay on the central Texas coast (Figs. 2 and 6). We used data from a 2014 airborne lidar survey of the Copano Bay area to produce a high-resolution DEM (Fig. 6) that we then used to examine subtle topographic features and guide the placement of boundaries between distinct lithologic units of the Beaumont Formation (sandy paleochannel features with subtle positive relief and mud-rich overbank or interchannel deposits in intervening topographic lows).

Lidar-derived elevations range from near sea level to about 18 m msl in the study area. In general, the land surface slopes toward the Gulf of Mexico to the southeast. Pleistocene Beaumont Formation muddy and sandy deposits occupy the higher elevations in the study area. This upland surface is incised by valleys cut by rivers such as the Mission River, which has built a Holocene delta in Mission Bay, and the Aransas River, which has built a Holocene delta in its valley at the western edge of Copano Bay (Fig. 6).

Prominent, elongated local highs (labeled H1 through H6 in Fig. 6) enter the study area from the north, west, and southwest. These highs on the uplands generally correlate with previously mapped sandy paleochannel facies in the Beaumont Formation. Their topographic expression revealed from lidar allows these features to be more accurately mapped and verified by subsequent sampling and geophysical measurements (Fig. 7) [26,27]. Other significant features can be seen in the high-resolution topographic data. A curvilinear, coast-parallel scarp (labeled "S" in Fig. 6) extends from the Pleistocene upland north of Mission Bay through the Mission River delta in the Holocene valley, marking the likely position of a previously unrecognized fault with probable recent movement. Sharp topographic boundaries on the southeast margin of a locally high feature in the southwest part of the map (H6, Fig. 6) may represent a former bay margin associated with the Pleistocene (Ingleside) barrier-island complex that likely formed

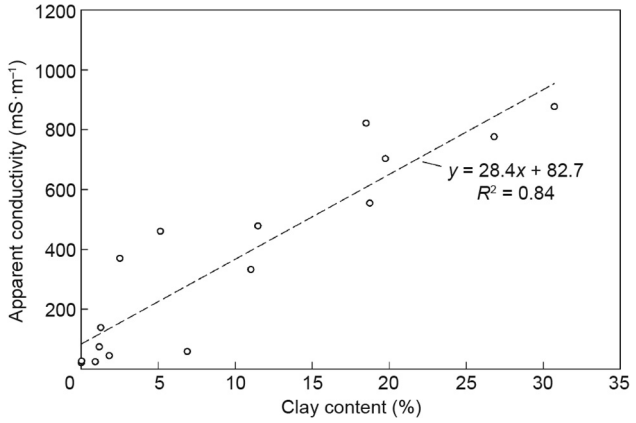

Fig. 5. Relationship between clay content (determined from borehole samples) and apparent conductivity (from geophysical logs) from depths above the water-saturation zone in two boreholes on the Pleistocene surface adjacent to the Nueces River valley (Fig. 2).

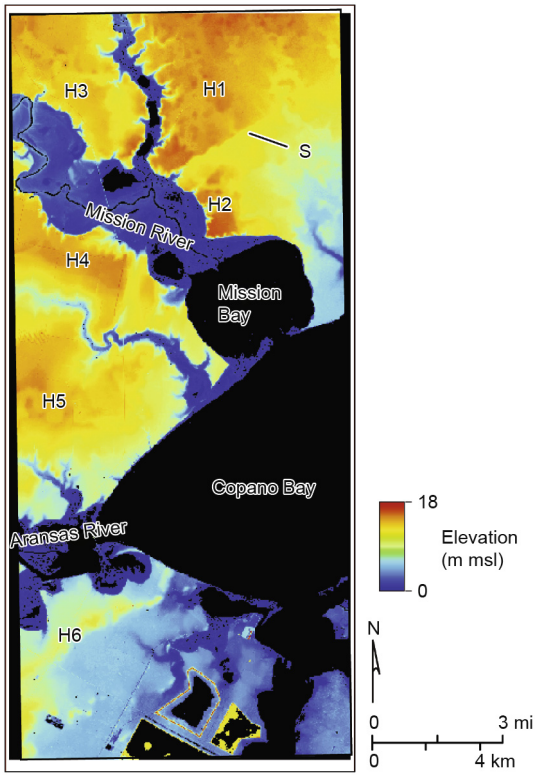

Fig. 6. DEM (1 m^2 cell size) of the Bayside and Mission Bay quadrangles, Copano Bay area, constructed from airborne lidar data acquired in 2014. Areas labeled H1 through H6 indicate local elevation highs that correspond to relatively sandy Pleistocene channel courses. Feature S denotes a scarp where there is an abrupt elevation change likely associated with an active fault.

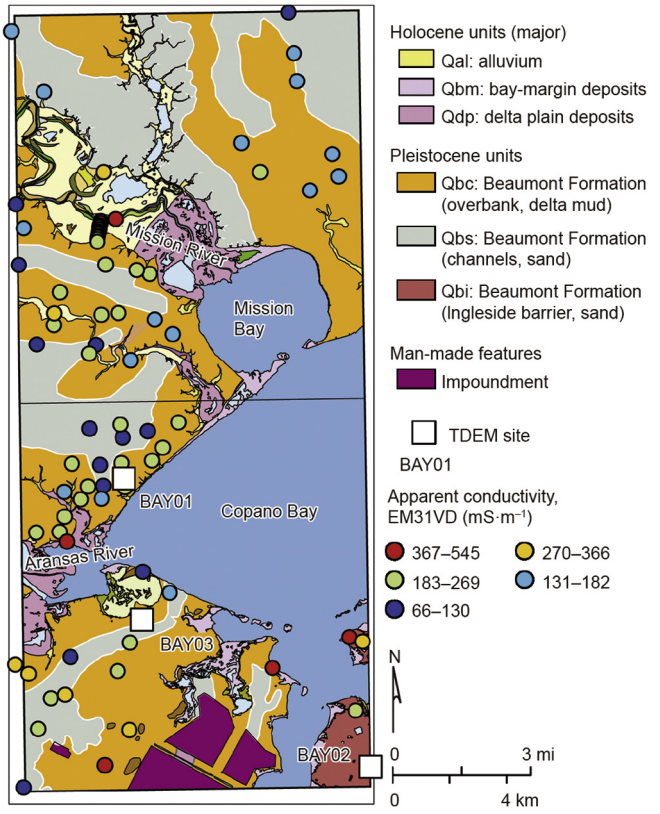

Fig. 7. Geologic map of the Bayside and Mission Bay quadrangles showing Quaternary fluvial, deltaic, and marine-influenced deposits mapped on the basis of geomorphic character expressed in a DEM produced from airborne lidar data, aerial photographs, and ground-based electrical conductivity measurements acquired using EM instruments. (Adapted from Refs. [26,27])

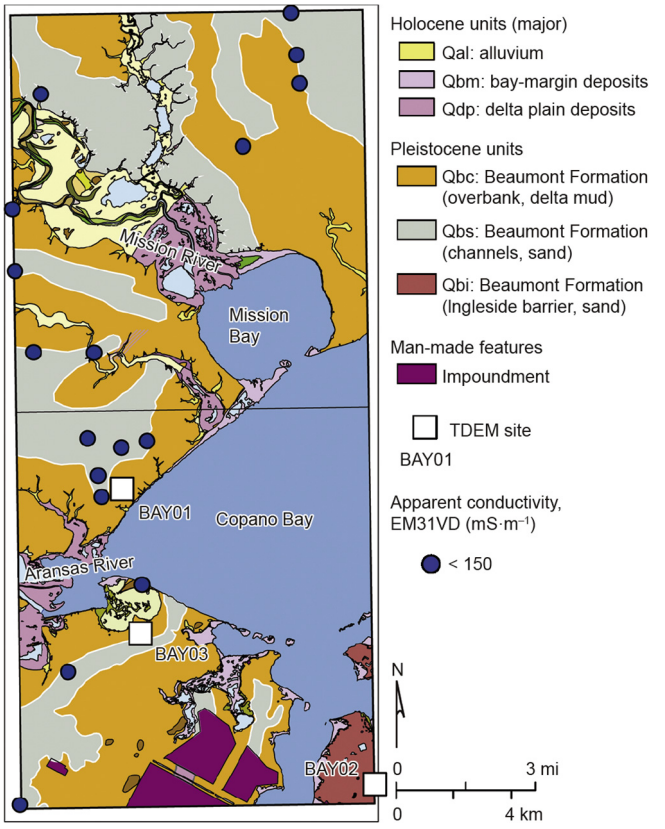

Fig. 8. Geologic map of the Bayside and Mission Bay quadrangles showing the spatial relationship between interpreted sandy channel deposits of the Beaumont Formation (Qbs) and the least conductive (less than 150 mS·m^{-1}) electrical conductivity measurements acquired using a Geonics EM31 in vertical dipole orientation.

during the most recent full interglacial period (oxygen-isotope stage 5) at about 100 ka [28–31].

5. Lithology from surface geophysics

Preliminary geologic mapping accomplished through interpretation of DEMs and aerial photographs can be verified and refined with surface geophysical measurements. We acquired ground conductivity measurements using an EM31 instrument at 83 sites within the study area and augmented those shallow-focused measurements with deeper TDEM soundings at three locations (Fig. 7). We used the ground conductivity measurements as a proxy for sand or clay content; higher conductivities were interpreted to be associated with clay-rich Pleistocene interchannel or overbank deposits (Qbc, Fig. 7), whereas low conductivities tended to occur on the subtle topographic highs where we mapped sandier Pleistocene paleochannel deposits (Qbs, Figs. 7 and 8). Low conductivities were also measured in the southeast corner of the study area, where the sand-rich deposits associated with the Pleistocene barrier-island complex (Qbi, Figs. 7 and 8) extend into the map area.

Horizontal and vertical dipole apparent conductivity measurements made using an EM31, while useful for distinguishing distinct surficial lithologic units and determining boundaries between them, provide little information about the depth and thickness of these units. Conductivity profiles determined from TDEM soundings can be used to estimate the thickness of surficial units, and perhaps the lithology and depths of underlying units, to depths of 100 m or more. The TDEM sounding BAY02, located on the Pleistocene barrier island, recorded a transient response to 2 ms after turnoff and yielded a four-layer model with a low fitting error of 1.6% root mean square (RMS) (Fig. 9). At this site, a low-conductivity (79 mS·m^{-1}) layer extends from 3 to 31 m below the surface, likely representing the dominantly sandy barrier-island complex. At TDEM site BAY01 (Fig. 7), near the margin of an interpreted sandy paleochannel within the Beaumont Formation, a three-layer conductivity model yielded a fitting error of 1.4% RMS (Fig. 9). Here, a 2.4 m thick, relatively resistive (41 mS·m^{-1}), likely sand-rich paleochannel unit of the Beaumont Formation overlies a highly conductive (728 mS·m^{-1}), likely clay-rich overbank, interdistributary, or estuarine unit that is 20 m thick. Below that, a more resistive (220 mS·m^{-1}) unit of unknown thickness likely represents another sandy unit deeper in the Beaumont Formation.

6. Vertical boundaries from borehole geophysics and sampling

Borehole samples, measurements, and direct observations provide a more detailed view of the subsurface and reveal critical geologic information, such as the presence of buried soil horizons that cannot be obtained from topographic, remote-sensing, or geophysical measurements. A cross-section constructed from geophysical logs and data from sediment samples from the four Nueces River valley boreholes (Figs. 2 and 10) reveals geologic complexity that reflects the influence of multiple periods of deposition, erosion, and soil formation that we expect to encounter in Quaternary coastal plain deposits in general, and in the Beaumont Formation and Lissie Formation on the lower Texas Coastal Plain in particular. The section is constructed from the upland (Beaumont Formation) south of the valley (borehole ND-05) through two boreholes (ND-07 and ND-06) on the Nueces River delta on the valley floor, and

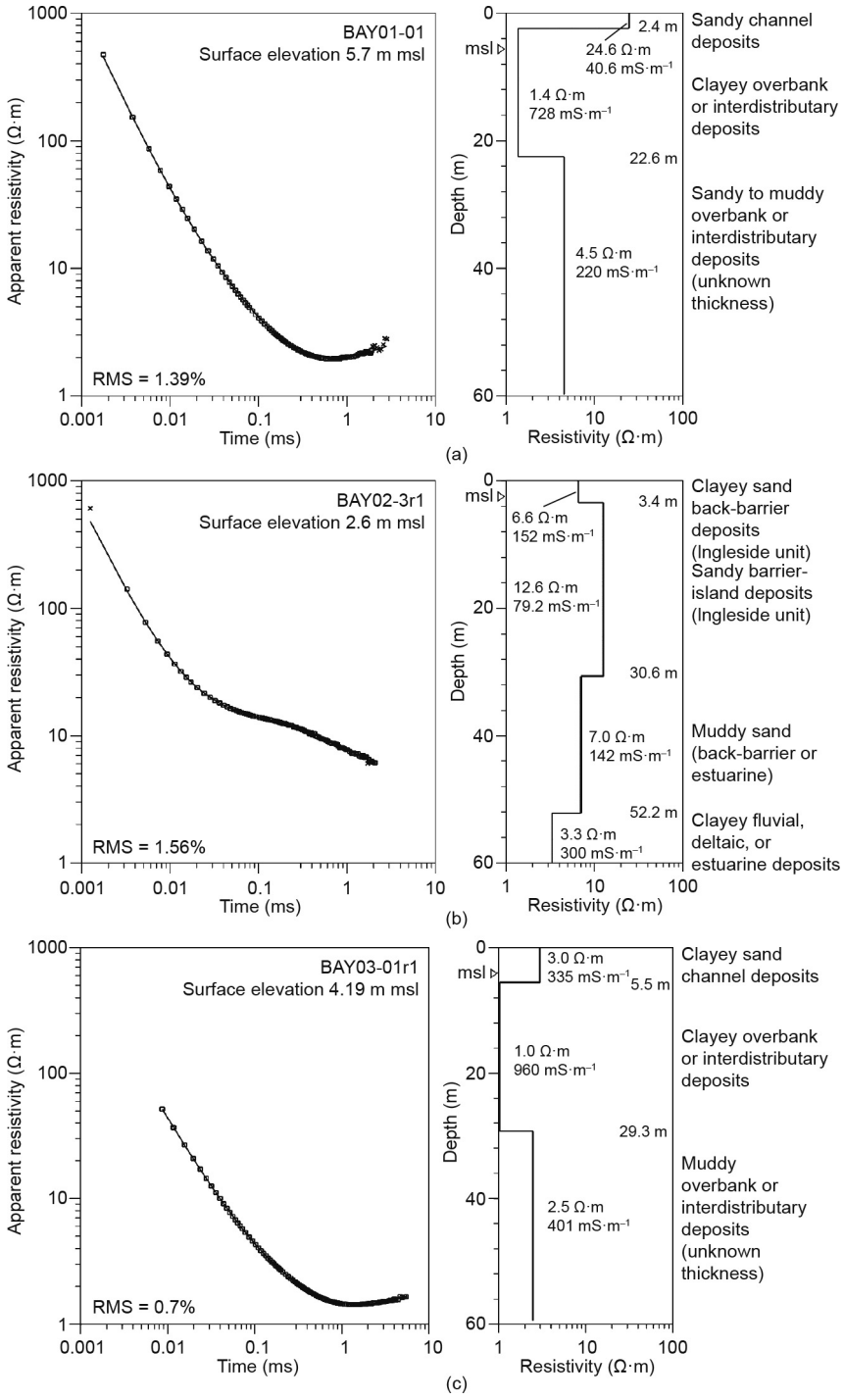

Fig. 9. TDEM soundings (a) BAY01, (b) BAY02, and (c) BAY03 acquired in the Copano Bay area (Fig. 7). At left are the apparent resistivities observed during the decay of the transient signal (individual points) and the transient decay predicted from the resistivity model shown at right (solid lines). The RMS values represent the percent difference between the observed and modeled values. The resistivity models on the right are also presented in conductivity units and are annotated with lithologic interpretations.

terminates on a mid-elevation fluvial terrace on the north side of the Nueces River valley (borehole ND-01). Each gamma log shows variations in count rates that are correlated to variations in clay content (similar to ND-06, Fig. 3). Sample descriptions from the boreholes include color, texture, and accessory information such as the presence of shell, carbonate nodules indicative of buried soil horizons, and soil slickensides indicative of vertisol development in clay-rich strata.

Using a combination of geophysical log character (gamma counts and conductivity), soil descriptions, and laboratory-measured textural information, the borehole data are interpreted to show that Pleistocene deposits border and underlie more recent deposits that partly fill the Nueces River valley. Holocene fluvial, deltaic, and estuarine (shell-bearing) deposits (Qal, Fig. 10) extend from the valley floor near sea level to a depth of 10–15 m, where older deposits (Qb_3–Qb_5, Beaumont Formation) with evidence of soil formation occur. On the upland south of the valley, two distinct buried soil horizons are evident at depths of 13 and 22 m, suggesting three episodes of deposition (Qb_3, Qb_2, and Qb_1 from oldest to youngest, Fig. 10) separated by periods of possible

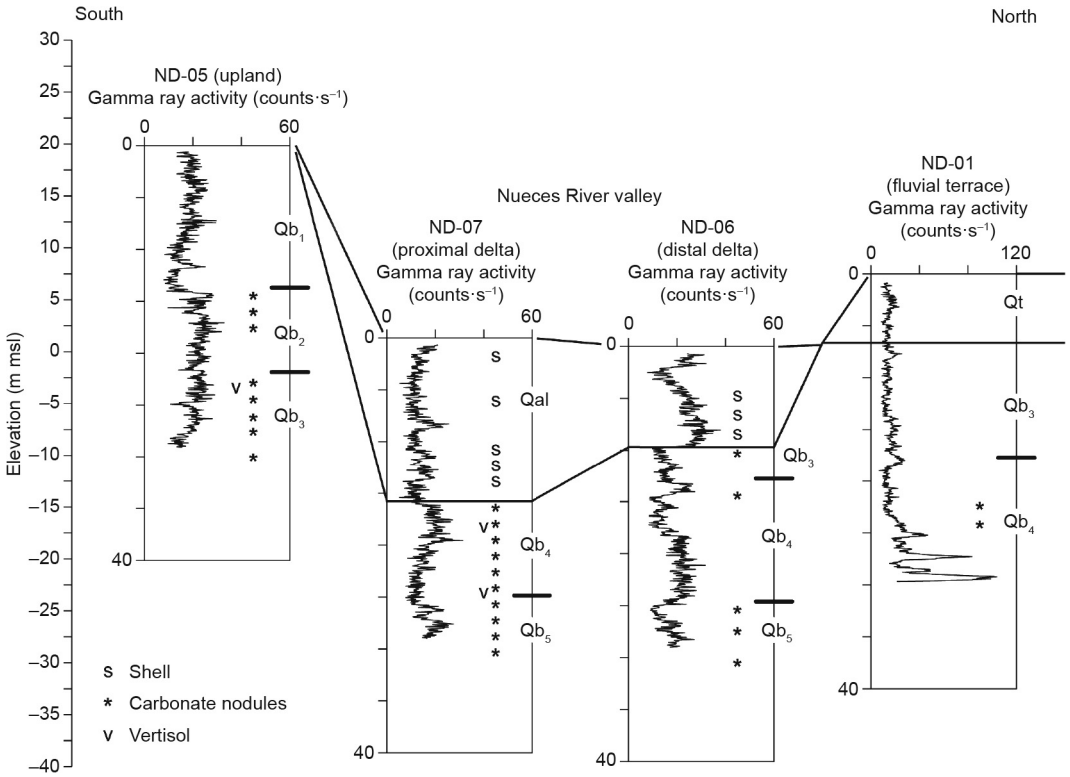

Fig. 10. Cross-section across the Nueces River valley constructed from gamma logs and lithologic data acquired in four boreholes upstream from Corpus Christi Bay (Fig. 2). Borehole ND-05 is on the Pleistocene Beaumont Formation south of the valley. Boreholes ND-07 and ND-06 are on the delta surface (Qal) on the valley floor. Borehole ND-01 is on a fluvial terrace (Qt) on the north side of the valley. Qb_1 through Qb_5 are interpreted to be distinct lithologic units within the Beaumont Formation, based on log response, sample descriptions, and textural analyses.

erosion and weathering. Only one of these boundaries (Qb_1 to Qb_2, Fig. 10) is evident from the geophysical log alone, which detects the lithologic change but not soil development.

On the north side of the valley, a sandy fluvial terrace about 7 m thick (Qt, Fig. 10) overlies older deposits that are interpreted to be part of the Beaumont Formation. It appears that the soil horizon atop the Beaumont Formation has been eroded, but a second soil horizon occurs at a depth of about 18 m. Buried soil horizons within the Beaumont Formation are also evident from borehole samples beneath the Holocene valley fill on the floor of the valley, where three distinct pedogenic carbonate nodule zones occur in borehole ND-06, and two occur in ND-07. Some of these features correspond with lithologic boundaries that could be interpreted from gamma or conductivity logs (Qal to Qb_3 in ND-06, Qal to Qb_4 in ND-07, and Qb_4 to Qb_5 in both, Fig. 10), but others are not clearly interpretable from geophysical data alone.

Taken together, and assuming lateral equivalence of strata across the Nueces River valley, there is evidence for as many as seven distinct Quaternary geologic units at depths of 0–30 m and between elevations of 20 and −25 m msl. These include the Holocene fluvial, deltaic, and estuarine deposits (Qal) that partly fill the valley, the elevated fluvial terrace sands (Qt) on the northern side of the valley, and the five units (Qb_1–Qb_5) separated by soil horizons and unconformities within the underlying Beaumont Formation (Fig. 10).

7. Conclusions

Advances in airborne lidar and geophysical instrumentation present an opportunity to better understand the lithologic and geologic complexity and heterogeneity present on the low-relief siliciclastic coastal plains that are common on passive continental margins worldwide. Using an example from the Texas Coastal Plain, high-resolution DEMs, aerial photographs, and surface geophysical measurements helped to delineate the boundaries of surficial geologic units and provided a general lithologic framework for subsurface units. Borehole geophysical data provided more detailed information on subsurface lithologic units, but did not detect important intraformational lithologic and pedologic boundaries that may correlate with major climatic and sea-level fluctuations that have occurred during the Quaternary period. These important boundaries can be inferred from geophysical log relationships and confirmed by judicious drilling and subsurface sampling. The overall approach to lithologic discrimination employs ① airborne lidar to produce high-resolution DEMs that can detect subtle topographic signatures of Quaternary depositional and erosional features; ② surface geophysical measurements to identify dominant lithology, distinguish surficial geologic units, and estimate the depths, thicknesses, and lithologies of subsurface units; ③ borehole geophysical measurements to establish the character and detailed lithologic framework of subsurface units; and ④ direct geological observation of subsurface samples to identify key erosional and pedogenic features. These methods are being used to gain a more complete understanding of the spatial distribution of the near-surface lithologic units that constitute the natural foundation for coastal-plain land use and infrastructure development, and of the relationship between Quaternary climatic and sea-level cycles and the depositional record on the Texas Coastal Plain. This approach is equally applicable to similar siliciclastic coastal plains found on passive continental margins worldwide.

Acknowledgments

The State of Texas Advanced Oil and Gas Resource Recovery (STARR) Program at the Bureau of Economic Geology,

The University of Texas at Austin, partly supported field and laboratory studies. This investigation complemented geologic mapping that was partly supported by the US Geological Survey (USGS) National Cooperative Geologic Mapping Program (G13AC00178). Bureau of Economic Geology staff John Andrews, Aaron Averett, Tiffany Caudle, John Hupp, and Kutalmis Saylam acquired and processed the airborne lidar data, and Todd Caldwell oversaw textural analyses of sediment samples. The manuscript benefited from review and comment by anonymous reviewers. Publication authorized by the director, Bureau of Economic Geology.

Compliance with ethics guidelines

Jeffrey G. Paine, Edward W. Collins, and Lucie Costard declare that they have no conflict of interest or financial conflicts to disclose.

References

[1] McNeill JD. Electrical conductivity of soils and rocks, technical note TN-5. Mississauga: Geonics, Ltd.; 1980.
[2] Bureau of Economic Geology. Geology of Texas map. Austin: Bureau of Economic Geology, The University of Texas at Austin; 1992.
[3] Hayes CW, Kennedy W. Oil fields of the Texas–Louisiana Gulf Coastal Plain. Report. Washington, DC: US Government Printing Office; 1903.
[4] Sellards EH, Adkins WS, Plummer FB. The geology of Texas, volume I: stratigraphy. Austin: Bureau of Economic Geology, The University of Texas at Austin; 1932.
[5] Price WA. Lissie Formation and the Beaumont clay in south Texas. Am Assoc Pet Geol Bull 1934;18(7):948–59.
[6] Price WA. Sedimentology and quaternary geomorphology of south Texas. Am Assoc Pet Geol Bull 1958;8:41–75.
[7] Metcalf RJ. Deposition of Lissie and Beaumont formations of Gulf Coast of Texas. Am Assoc Pet Geol Bull 1940;24:693–700.
[8] Doering JA. Review of quaternary surface formations of Gulf Coast region. Am Assoc Pet Geol Bull 1956;40:1816–62.
[9] Aronow S. Nueces River delta plain of pleistocene Beaumont Formation, Corpus Christi region, Texas. Am Assoc Pet Geol Bull 1971;55:1231–48.
[10] Brewton JL, Brown LF Jr, McGowen JH. Geologic atlas of Texas, Corpus Christi sheet. Austin: Bureau of Economic Geology, The University of Texas at Austin; 1975.
[11] Brown LF Jr, Brewton JL, McGowen JH, Evans TJ, Fisher WL, Groat CG. Geologic atlas of Texas, Beeville-Bay City sheet. Austin: Bureau of Economic Geology, The University of Texas at Austin; 1987.
[12] Shackleton NJ, Opdyke ND. Oxygen isotope and paleomagnetic stratigraphy of Equatorial Pacific core V28–238: oxygen isotope temperatures and ice volumes on a 10^5 and 10^6 year scale. Quat Res 1973;3(1):39–55.
[13] Shackleton NJ, Opdyke ND. Oxygen-isotope and paleomagnetic stratigraphy of Pacific core V28–239: late Pliocene to latest Pleistocene. Geol Soc Am 1976;145:449–64.
[14] Imbrie J, Hays JD, Martinson DG, McIntyre A, Mix AC, Morley JJ, et al. The orbital theory of Pleistocene climate: support from a revised chronology of the marine ^{18}O record. Milankovitch Clim 1984;126(1):269–305.
[15] Lorius C, Jouzel J, Ritz C, Merlivat L, Barkov NI, Korotkevich YS, et al. A 150,000-year climatic record from Antarctic ice. Nature 1985;316(6029):591–6.
[16] Robin G. Contrasts in Vostok core—changes in climate or ice volume? Nature 1985;316:578–9.
[17] Lisiecki LE, Raymo ME. A Pliocene-Pleistocene stack of 57 globally distributed benthic $\delta^{18}O$ records. Paleoceanography 2005(20):PA1003.
[18] Paine JG, Caudle T, Andrews J, Averett A, Hupp J, Saylam K, et al. Shoreline movement in the Copano, San Antonio, and Matagorda Bay systems, central Texas coast, 1930s to 2010s. Final Report. Austin: Bureau of Economic Geology, The University of Texas at Austin; 2016. Contract No.: 13-258-000-7485.
[19] Parasnis DS. Principles of applied geophysics. 5th ed. New York: Chapman and Hall; 1986.
[20] Frischknecht FC, Labson VF, Spies BR, Anderson WL. Profiling using small sources. In: Nabighian MN, editor. Electromagnetic methods in applied geophysics-applications, part A and part B. Tulsa: Society of Exploration Geophysicists; 1991. p. 105–270.
[21] West GF, Macnae JC. Physics of the electromagnetic induction exploration method. In: Nabighian MN, editor. Electromagnetic methods in applied geophysics-applications, part A and part B. Tulsa: Society of Exploration Geophysicists; 1991. p. 5–45.
[22] McNeill JD. Electromagnetic terrain conductivity measurement at low induction numbers. Report. Mississauga: Geonics, Ltd.; 1980.
[23] Kaufman A, Keller GV. Frequency and transient soundings. In: Kaufman AA, editor. Methods in geochemistry and geophysics. Amsterdam: Elsevier; 1983. p. 685.
[24] Spies R, Frischknecht FC. Electromagnetic sounding. In: Nabighian MN, editor. Electromagnetic methods in applied geophysics-applications, part A and part B. Tulsa: Society of Exploration Geophysicists; 1991. p. 285–386.
[25] Paine JG, Goldsmith RS, Scanlon BR. Electrical conductivity and gamma-ray response to clay, water, and chloride content in fissured sediments, Trans-Pecos Texas. Environ Eng Geosci 1998;4(2):225–39.
[26] Paine JG, Collins EW. Geologic map of the Bayside quadrangle: Aransas Delta and Copano Bay area, Texas Gulf of Mexico Coast. Austin: Bureau of Economic Geology, The University of Texas at Austin; 2014.
[27] Paine JG, Collins EW. Geologic map of the Mission Bay quadrangle: Mission Delta and Copano Bay area. Austin: Bureau of Economic Geology, The University of Texas at Austin; 2014.
[28] Paine JG. Subsidence of the Texas coast: inferences from historical and late Pleistocene sea levels. Tectonophysics 1993;222(3–4):445–58.
[29] Otvos EG, Howat WE. South Texas Ingleside barrier; coastal sediment cycles and vertebrate fauna; late Pleistocene stratigraphy revised. GCAGS Transa 1996;46:333–44.
[30] Otvos EG. Numerical chronology of Pleistocene coastal plain and valley development; extensive aggradation during glacial low sea-levels. Quat Int 2005;135(1):91–113.
[31] Simms R, Anderson JB, DeWitt R, Lambeck K, Purcell A. Quantifying rates of coastal subsidence since the last interglacial and the role of sediment loading. Global Planet Change 2013;111:296–308.